LIQUID CRYSTALS
2020, VOL. 47, NO. 2, 238–247
https://doi.org/10.1080/02678292.2019.1641854

Taylor & Francis
Taylor & Francis Group

Controlling morphological and electro-optical properties via the phase separation in polymer/liquid-crystal composite materials

Ke Li[a], Haodong Jiang[a], Ming Cheng[a], Yifei Li[a], Zhen Yin[a], Dan Luo[a], Xiao Wei Sun[a,b] and Yan Jun Liu[a,b]

[a]Department of Electrical and Electronic Engineering, Southern University of Science and Technology, Shenzhen, China; [b]Shenzhen Planck Innovation Technologies Pte Ltd, Shenzhen, Longgang, China

ABSTRACT

The polymer/liquid-crystal composite materials have been extensively studied for their potential applications. Various optical devices based on this composite material have been proposed and realised. The device performance is highly dependent on the phase separation of this composite material. Here, we investigate the photopolymerisation-induced phase separation in this composite material. Depending on the mass ratios between the polymer and the liquid crystal, the phase separation can be well controlled and subsequently affect the morphological and electro-optical properties. At a fixed ratio, we can realise either phase-separated composite films or conventional polymer-dispersed liquid crystal films with completely different optical properties. By carefully controlling the exposure conditions, the morphologies and electro-optical properties have been studied and optimised in details. With in-depth studies and optimisation, the photopolymerisation-induced phase separation technique could be utilised to realise many different optical functions based on the polymer/liquid-crystal composite materials.

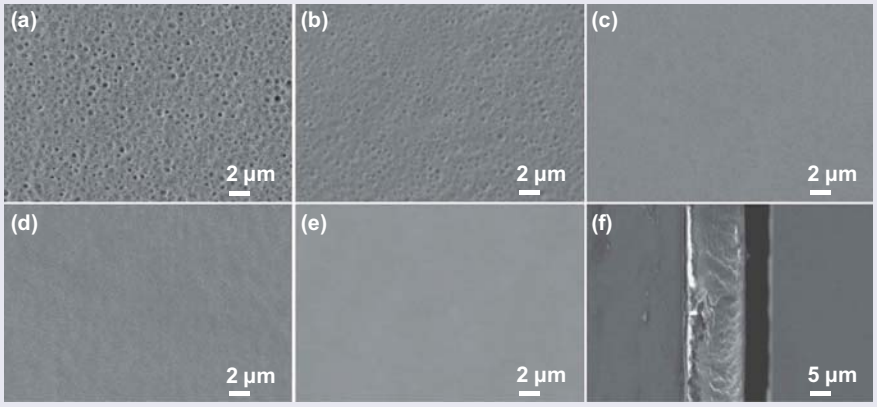

Great morphological changes demonstrated by the NOA65/E7 samples that were fabricated at different temperatures of (a) 30°C, (b) 35°C, (c) 40°C, (d) 45°C, and (e) 50°C with the fixed exposure intensity of 10 mW/cm^2. (f) Cross-sectional view of the corresponding sample (e).

ARTICLE HISTORY
Received 24 April 2019
Accepted 7 July 2019

KEYWORDS
Photopolymerisation; phase separation; morphology; electro-optical properties

1. Introduction

The polymer/liquid-crystal (LC) composite materials have been extensively studied for their many potential applications [1–7]. Various optical devices based on this composite material have been proposed and realised [4,8–16]. Up to date, researchers have tried different approaches to achieve the well phase-separated polymer and LC domains. The phase separation approaches mainly include solvent-induced phase separation [17], polymerisation-induced phase separation [18–20], temperature-induced phase separation [21–23], Fringing-field-induced phase separation [24]. Polymerisation-induced phase separation can be achieved by thermal polymerisation, electron beam polymerisation, or photopolymerisation [25–27]. Among them, photopolymerisation-induced phase separation (PIPS) stands out with many advantages including easy control, high resolution, cost-effectiveness. Meanwhile, it is also convenient to study the dynamic evolution of the fabrication process so as to analyze the internal relationship between fabrication conditions and optical performance of the sample [28,29]. With well-controlled phase separation between the LC and the polymer, one can achieve various phase-separated structures for different applications, such

CONTACT Yan Jun Liu yjliu@sustech.edu.cn

as polymer-dispersed liquid crystal (PDLC) [30], polymer-stabilised liquid crystal (PSLC) [31,32], phase-separated composite films (PSCOF) [33]. With a photomask, one can even design and achieve much more complex phase-separated structures with different optical functions like light valve, light steering, and phase condenser [34,35]. With advantageous features of cost-effective fabrication, easy integration, and stimuli-responsive tunability, the PIPS-enabled optical devices based on the polymer/LC composite materials could play an important role in future development of active photonic devices.

The PDLC and PSCOF structures are essentially fabricated based on similar composite materials but their optical functions are quite different. For the PDLC structure [36–46], LCs exist in the format of droplets inside the polymer matrix. Upon light incidence, these LC droplets will strongly scatter the incoming light due to the index mismatch between the LC droplets and the polymer, resulting in an opaque state. Once an external stimulus is applied, the LC molecules in each droplet will realign along the field direction and then meet the index match condition, leading to a transparent state. While for the PSCOF structure [47–49], the polymer and the LCs are separated into two adjacent uniform layers. The configuration of the optic axis in the LC layer can be pretreated with an alignment layer on the substrate closest to the LC layer. The working mechanism of PSCOF devices relies on the direction changes of the optic axis under an external electric field, as in conventional LCDs.

From the aforementioned discussion, the morphological and electro-optical properties of the PDLC and PSCOF structures are highly dependent on the phase separation of the polymer/LC composite material. While the PDLC and PSCOF structures have been extensively studied, respectively, little effort has been put to investigate the phase separation using the same composite material. In this work, we investigate the morphological and electric-optical properties of PIPS-fabricated samples based on the polymer/LC composite material. Depending on the mass ratios between the polymer and the LC, the phase separation can be well controlled and subsequently affect the morphological and electro-optical properties. At certain ratios, we can realise either PSCOF or PDLC films with completely different optical performance. By carefully controlling the exposure conditions, such as exposure intensity and temperature, the morphologies and electro-optical properties have been studied and optimised in details. With in-depth studies and optimisation, the PIPS technique could be utilised to realise many different optical functions based on the polymer/LC composite materials.

2. Experimental

2.1. Materials

In our experiments, the polymer/LC composite material used consists of a nematic LC, E7 (Jiangsu Hecheng Display Co., Ltd.) and an optical adhesive, NOA 65 (Norland Products, Inc.). The LC E7 is a mixed material with 51% 5CB, 25% 7CB, 16% 8OCB, 8% 5CT. It has a clearing point of 59.6°C and a high anisotropy with its ordinary and extraordinary refractive indices of n_o = 1.517 and n_e = 1.741, respectively, at the wavelength of 589 nm and the temperature of 20°C. The NOA65 is a mixture of trimethylolpropane diallyl ether, trimethylolpropane tris thiol, isophorone diisocyanate ester and a benzophenone photoinitiator [50]. Its refractive index is 1.524, which matches well with n_o of E7. All these materials were used without any further purification.

2.2. Sample preparation

E7 and NOA65 were mixed together at 60°C and stirred at 500 rpm/min for 2 h. In the NOA65/E7 composite material, the mass ratio of E7 was gradually varied from 30 wt% to 60 wt% with the step size of 10 wt%. The mixed syrup was then injected a LC cell using the capillary action at room temperature (25°C). The LC cell was assembled using two pieces of indium-tin-oxide (ITO) glass substrates with the thickness of ~20 μm. A UV light beam from an Ar^+ laser operating at 363 nm (Innova 306C, Coherent, USA) was used to irradiate the samples for 1 min with different exposure intensities. The exposure temperature was also controlled to vary from room temperature to 60°C with the heating rate of 5°C/min using a temperature controller (mK2000, Instec, Inc. USA).

2.3. Characterisation

The morphologies of the PDLC and PSCOF samples were characterised using the field emission scanning electron microscopy (FESEM) (GeminiSEM 300–71-10, Zeiss, Germany) and the polarizing optical microscope (POM) (Nikon 'pi', Japan). The electro-optical properties were measured by a LC electro-optic complex tester equipped with a white light source (ZKY-LCDE0-2, Chengdu Shijizhongke Equipment Co., Ltd.). The samples were driven by a square wave voltage with a frequency of 1 KHz, which was generated by a signal function generator (DG4102, Rigol, China) followed by 50× magnification using a power amplifier (PZD350A, Trek, USA). The response time was measured using an oscilloscope (DPO2024, Tektronix, USA).

3. Results and discussion

For the NOA65/E7 composite material, upon UV light exposure, the photoinitiator inside the NOA65 will produce free radicals that further induce the monomer to polymerise and then form crosslinking polymer matrix. Meanwhile, the LC molecules will start to nucleate and then grow into the droplets due to the photopolymerisation-induced diffusion and counter-diffusion. Thus, it is straightforward that the photopolymerisation process is highly dependent on the exposure conditions. We studied and compared the effect of exposure intensity and temperature on the size of LC droplets inside PDLC films. Figure 1 shows the typical morphologies of PDLC samples fabricated at different intensities with the NOA65 and E7 mass ratio of 1:1. It is worth noting that the morphologies (Figure 1(a–c)) are observed under FESEM with the LC cell decapped and the LCs washed away by ethyl alcohol. Judging from the holes that are originally occupied by the LC droplets, the size of the LC droplets can be statistically estimated, as shown in Figure 1(d–f). We can see that with the exposure intensity increased from 10 mW/cm^2 to 20 mW/cm^2, the size of LC droplets decreases dramatically from 0.89 μm to 0.32 μm. This can be well explained by the fact that the higher the exposure intensity, the faster the polymerisation rate. As known, the morphology of PDLC can be affected by many factors, such as the polymerisation rate, the diffusion rate, monomer ratio, and so on [51]. The polymerisation rate is greatly dependent on the intensity of the exposure light [52]. Therefore, the high exposure intensity will result in the rapid polymerisation locally, hence leaving the LC molecules insufficient time and limited room to grow into a big droplet. In contrast, the low exposure intensity causes the slow polymerisation so that the LC molecules get enough time and room to grow into a big droplet. Therefore, macroscopically, the rate of the photopolymerisation-induced diffusion and counter-diffusion plays a critical role on the formation of the morphology in the polymer/LC composite materials.

As known, the diffusion rate of the LC has a strong dependence on its viscosity, which is further highly temperature-dependent. Hence, we further investigated the temperature effect on the morphological properties. Figure 2 shows the typical morphologies of the fabricated samples under the exposure temperatures varying from 30°C to 50°C with the step size of 5°C at the exposure intensity of 10 mW/cm^2. We can clearly see from Figure 2(a,b) that the size of the LC droplets decreases as the exposure temperature increases, which is mainly caused the increase of the diffusion rate of LC and polymer. With the further increase of the exposure temperature, we can see that there are no obvious LC droplets formed in the polymer matrix. Interestingly, a much smooth polymeric surface is formed when the temperature is larger than 40°C (see Figure 2(c–e)). This indicates that the polymer and the LCs may form completely

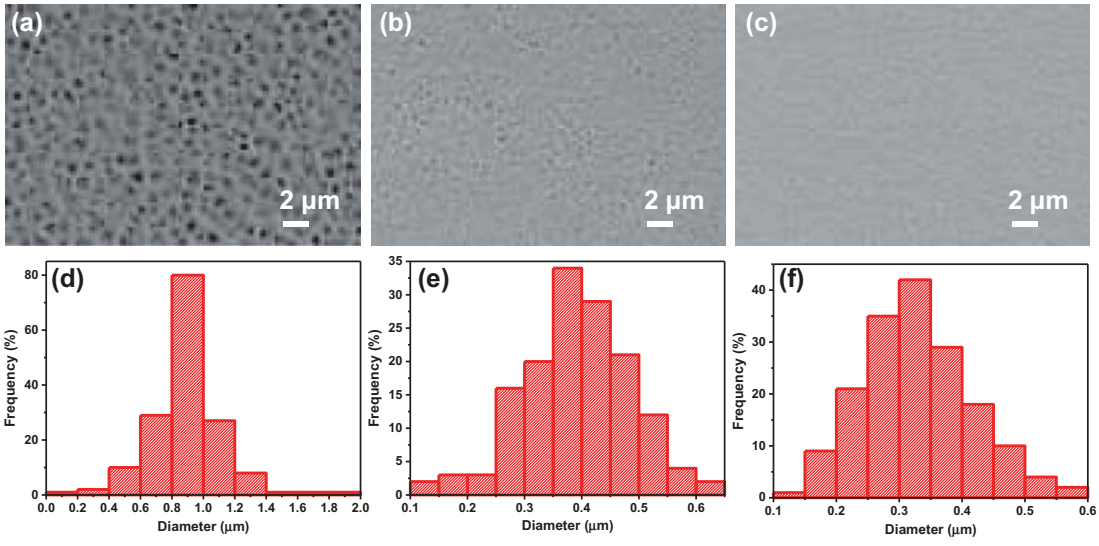

Figure 1. (Colour online) Typical morphologies (a–c) and corresponding histograms (d–f) of the LC droplet size distribution in the polymer matrix for the fabricated PDLC samples with the exposure intensities of (a, d) 10, (b, e) 15, and (c, f) 20 mW/cm^2 at room temperature, respectively.

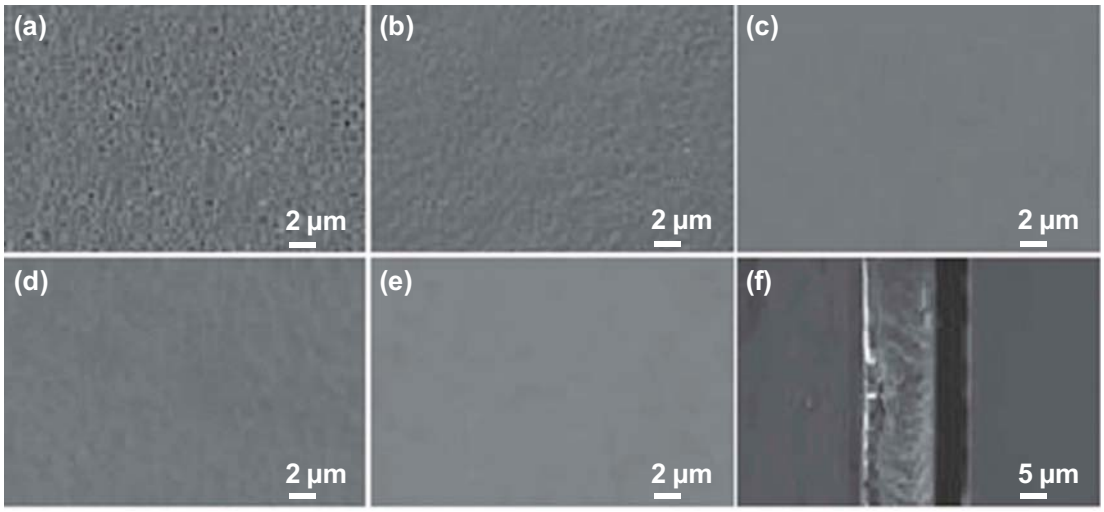

Figure 2. Morphologies of NOA65/E7 samples fabricated at the temperature of (a) 30°C, (b) 35°C, (c) 40°C, (d) 45°C, and (e) 50°C with the fixed exposure intensity of 10 mW/cm^2. (f) Cross-sectional view of the corresponding sample (e).

separated layers via the phase separation (i.e. PSCOF). To confirm this, we therefore checked the cross-sectional morphology of the sample. Figure 2(f) shows the cross-sectional view of the corresponding sample fabricated at the exposure temperature of 50°C. It is obvious that separated adjacent polymer layer (bright region) and LC layer (dark region) are formed inside the LC cell. The thicknesses of the polymer and LC layers are measured to be 14 and 6 μm, respectively. It is well known that as the exposure temperature increases, the viscosities of both the polymer and the LC decrease, resulting in high molecular mobility. Along the direction of the cell thickness, due to the absorption of the NOA65/E7 composite material, an intensity gradient of the UV exposure light will be created from one side nearest (the top of the LC cell) to the incoming light to the other side farthest (the bottom of the LC cell). As a result, NOA 65 will firstly undergo polymerisation at the top of the cell. The bottom NOA65 will diffuse towards the top and the LCs will be expelled into the bottom of the cell. With deliberate exposure conditions, long enough UV exposure eventually consumes all the NOA65 monomers and causes LCs to move out of the polymerised volume [53]. Finally, a PSCOF structure inside the LC cell is formed. The texture of the formed PSCOF structure was further checked under the POM, as shown in Figure 3. Completely different from the PDLC structure, a locally-aligned domain texture can be observed, which is mainly caused by the volume driving force generated during the temperature quench after removing the sample from the hot stage according to the Allen-Cahn theory [54,55]. Alternate bright and dark regions are demonstrated by rotating the PSCOF sample counterclockwisely with the rotation step size of 60°, confirming the multi-domain textures inside the PSCOF. It is worth noting that with a proper pretreatment of the cell, a uniformly aligned LC layer could be achieved in the PSCOF structure.

The above experimental results show that the rate of phase separation can be deliberately controlled to achieve the completely different morphologies in the NOA65/E7 composite material system. It is also expected that the phase-separated structures will possess morphology-dependent electro-optical properties. Figure 4(a) shows the normalised optical transmittance versus the applied voltage for the samples fabricated at the exposure intensity of 10, 15, and 20 mW/cm^2, respectively. From the electro-optical curves, we can achieve the threshold (V_{th}) and switching (V_{s}) voltages, which define as the applied voltages making the transmittance reach 10% and 90%, respectively. As reported previously [40], the threshold (V_{th}) and switching (V_{s}) voltages can be written as

$$V_{th}\,\alpha\,\frac{d_0}{3a}\left(\frac{\sigma_2}{\sigma_1}+2\right)\left[\frac{K(l^2-1)}{\Delta\varepsilon}\right]^{1/2} \tag{1}$$

$$Vs\,\alpha\,\frac{d_0}{3a}\left[\frac{4\pi K(l^2-1)}{\Delta\varepsilon}\right]^{1/2} \tag{2}$$

where d_0 is the sample thickness, $l = a/b$ is the aspect ratio of the LC droplet with a and b being the lengths of the semi-major and semi-minor axes of the droplet, σ_1 and σ_2 are the conductivity of

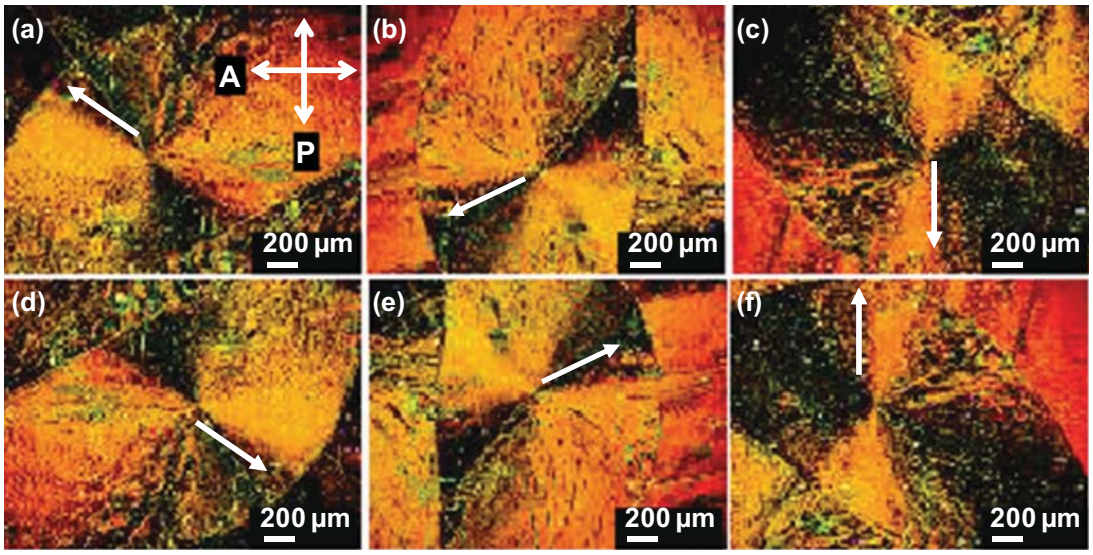

Figure 3. (Colour online) A group of POM images (a–f) of the PSCOF sample taken by rotating the sample counterclockwisely with the rotation step size of 60°. The inset in (a) labels the crossed polarisation directions given by the polarizer (P) and analyzer (A).

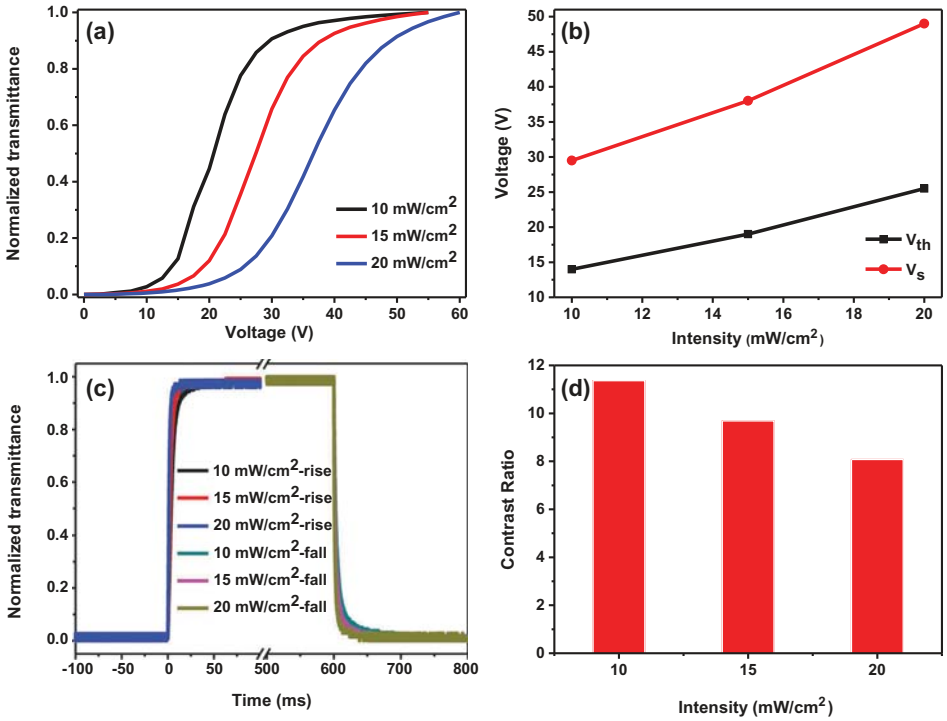

Figure 4. (Colour online) Electro-optical properties of three PDLC samples fabricated at room temperature with the exposure intensity of 10, 15, and 20 mW/cm^2, respectively. (a) Normalised transmittance versus the applied voltages; (b) Threshold and switching voltages versus the exposure intensities; (c) Measured response time at the switching voltage; (d) Measured CR at different exposure intensities. All the data were achieved at room temperature.

polymer and LC, respectively, K is the deformation constant, $\Delta\varepsilon$ is the anisotropy in the dielectric constant. From Equations (1) and (2), low threshold and switching voltages can be achieved for PDLC films with large LC droplets. It can be also derived that the slope of the switching voltage is steeper than that of the threshold voltage, as shown in Figure 4(b). The response time can be described as

$$\tau_{on}^{-1} = \frac{1}{\left[\frac{1}{\gamma_1}\left(\Delta\varepsilon \cdot E^2 + \frac{K(l^2-1)}{a^2}\right)\right]} \tag{3}$$

where γ_1 is the rotational viscosity coefficient. When the applied voltage is large, Equation (3) can be re-written as:

$$\tau_{on} = \frac{\gamma_1}{\Delta\varepsilon \cdot E^2} \tag{4}$$

$$\tau_{off} = \frac{\gamma_1 \cdot a^2}{K(l^2 - 1)} \tag{5}$$

Figure 4(c) shows the measured response time that is summarised in Table 1. Note that the response time is the sum of the rise and fall time. From Equations. (4) and (5), the rise time is inversely proportional to the square of the applied electric field (i.e. the switching voltage), while the fall time is proportional to the size of the LC droplets. As we can see from Figure 1, the size of the LC droplets decreases as the exposure intensity increases. Experimentally measured results from Figure 4 and Table 1 show that both the rise and the fall time decreases due to the increased switching voltage and the reduced size of the LC droplets, respectively, resulting in total decrease of the response time.

Contrast ratio (CR) is another important parameter for PDLC that is defined as

Table 1. The response time of different irradiation intensity.

Intensity (mW/cm^2)	Rise time (ms)	Fall time (ms)	Response time (ms)
10	10.84	16.47	27.31
15	7.19	10.63	17.82
20	3.45	5.92	9.37

$$CR = \frac{T_{\max}}{T_{\min}} \tag{6}$$

where $T_{\max}$ and $T_{\min}$ are the highest and lowest transmittance of the PDLC film before and after applying the driving voltage. For the NOA65/E7 composite material, with the exposure intensity increasing from 10 to 20 mW/cm^2, the LC droplets become small gradually, leading to weak scattering and high transmittance. As a result, CR decreases gradually from 12.26 to 8.07, as shown in Figure 4(d).

Figure 5 shows the electro-optical measurement of the samples fabricated at different exposure temperatures. From Figure 5(a), we can see that as the temperature increases from 25°C to 45°C, the transmission curves have a gradual right-shift, indicating increased threshold and switching voltages, as shown in Figure 5(b). This can be ascribed to the

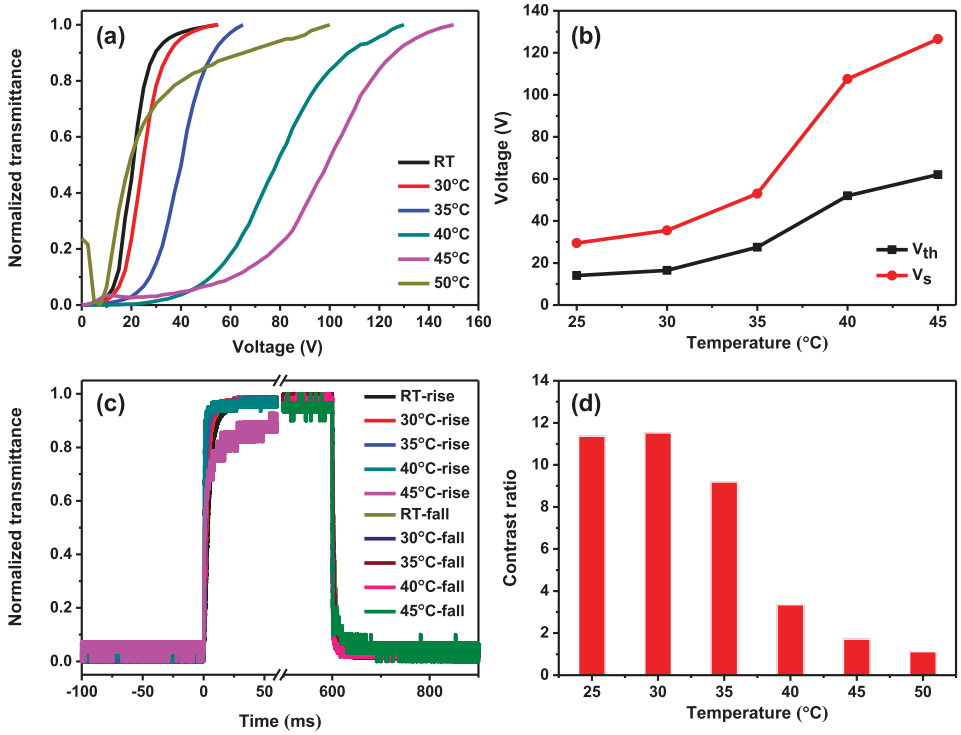

Figure 5. (Colour online) Electro-optical properties of polymer/LC composite samples at different exposure temperatures from room temperature to 50°C with the step size of 5°C. (a) Normalised transmittance versus the applied voltages; (b) Threshold and switching voltages versus the exposure temperature; (c) Measured response time at the switching voltages; (d) Measured CR at different exposure temperatures. All the samples were fabricated at the same exposure intensity of 10 mW/cm^2 and measured at room temperature.

reduced size of the LC droplets, as shown in Figure 2. Astonishingly, when the exposure temperature rises to 50°C, the transmission curve shifts back to the left, showing a greatly reduced threshold voltage. This is caused by the structural change from PDLC to PSCOF. In PSCOF, the LCs exist in layered bulk state instead of droplet form. Figure 5(c) shows the measured response time that is summarised in Table 2. We can see that as the temperature increases from RT to 40°C, the size of the LC droplets decreases, and the response time including both the rise and fall time will decrease due to the high surface-to-volume ratio. When the structure transforms from PDLC to PSCOF above 45°C, the layered bulk LC demonstrates response time at least one order magnitude slower than PDLC case. It is worth mentioning that we did not measure the response time for the case at the temperature of 50°C as the optical transmittance does not change much upon applying a voltage. Figure 5(d) shows the measured contrast ratios of the different samples. For the PDLC structure, the contrast ratio decreases dramatically from ~11 to ~3 as the droplet size decreases. For the PSCOF structure, since the optical transmittance does not change much before and after applying a voltage, leading to a low contrast ratio of only ~1, as shown in Figure 5(d).

Table 2. The measured response time of the samples fabricated at different exposure temperatures with the same exposure intensity of 10 mW/cm$^{2.}$

Temperature (°C)	Rise time (ms)	Fall time (ms)	Response time (ms)
25	10.84	16.47	27.31
30	8.15	9.84	17.99
35	5.27	5.41	10.68
40	1.93	2.8	4.73
45	216.53	16.64	233.17

We further investigated the effect of the LC concentration in the mixture solution of NOA65 and E7 on the PSCOF formation, and found that PSCOF structure can be obtained by adjusting the exposure temperature when the LC concentration is in the range of 30–60 wt%, as shown in Figure 6(a). The transition temperature from PDLC to PSCOF increases with the increase of the LC concentration. This could be mainly ascribed to the decreased viscosity of the composite material caused by the increased exposure temperature. Figure 6(a) provides an empirical boundary in terms of the LC concentrations and exposure temperatures to achieve the PDLC and

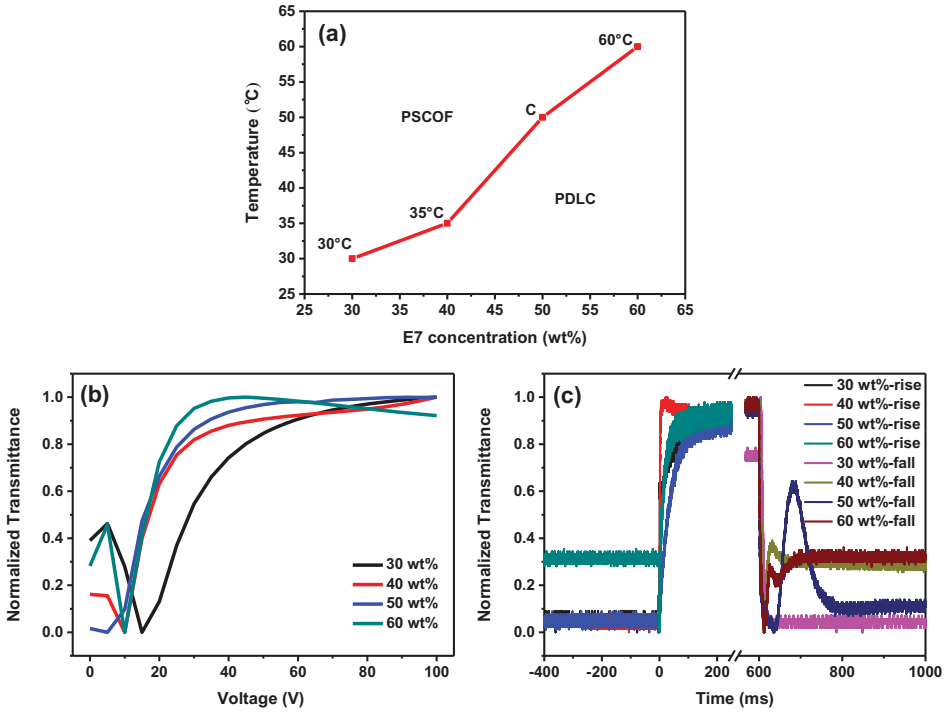

Figure 6. (Colour online) (a) The transition temperature point from PDLC to PSCOF as a function of the LC concentration in the NOA65/E7 composite material at the exposure intensity of 10 mW/cm^2. Measured electro-optical properties of four typical PSCOF samples: (b) normalised transmittance versus the applied voltages, and (c) response time at the switching voltages. The four typical PSCOF samples were fabricated with the LC (E7) concentrations and exposure temperatures being 30 wt% at 30°C, 40 wt% at 35°C, 50 wt% at 50°C, and 60 wt% at 60°C, respectively.

PSCOF, respectively. With a relatively low exposure intensity, the phase separation of the polymer and the LCs could reach a deliberate equilibrium, forming a bilayer PSCOF structure. With this empirical boundary, we have fabricated four typical PSCOF samples with different LC concentrations and exposure temperatures and then measured their corresponding electro-optical properties, as shown in Figure 6(b,c). Figure 6(b) shows the normalised transmittance as a function of the applied voltages of the PSCOF samples. As the LC concentration increases from 30 to 60 wt%, the transmission curves show a left-shift, indicating decreased threshold and switching voltages. Figure 6(c) shows the measured response time correspondingly. The response times for all samples are about few hundred milliseconds, showing similar response as the bulk LCs.

4. Conclusion

In summary, we have investigated morphological and electro-optical properties via the PIPS technique in the NOA65/E7 composite material. At certain mass ratios, we have achieved both PDLC and PSCOF structures with completely different electro-optical properties. For PDLC, the exposure intensity has a strong effect on the morphological and electro-optical properties. As the exposure intensity increases, the LC droplets decrease, resulting in fast response time, high threshold and switching voltages, and low CR, and vice versa. While for PSCOF, the exposure temperature plays a critical role. The high temperature causes the reduced viscosities of both the polymer and the LC, resulting in high molecular mobility. With deliberate exposure conditions, the phase separation can be well controlled and subsequently affect the morphological and electro-optical properties. With in-depth studies and optimisation, the PIPS technique could be utilised to realise many different optical functions based on the polymer/LC composite materials.

Disclosure statement

No potential conflict of interest was reported by the authors.

Funding

This work was supported by the Shenzhen Science and Technology Innovation Commission [JCYJ20170817111349280 and KQTD2016030111203005];Natural Science Foundation of Guangdong Province [2017A030313034 and 2018A030310224]; Guangdong Innovative and Entrepreneurial Research Team Program [2017ZT07C071];National Natural Science Foundation of China [61805113].

References

[1] Bunning TJ, Natarajan LV, Sutherland RL. Holographic polymer-dispersed liquid crystals (H-PDLCs). Annu Rev Mater Sci. 2000;30:83–115.
[2] Ouskova E, De Sio L, Vergara R, et al. Ultra-fast solid state electro-optical modulator based on liquid crystal polymer and liquid crystal composites. Appl Phys Lett. 2014;105:231122.
[3] Kumano N, Seki T, Ishii M, et al. Multicolor polymer-dispersed liquid crystal. Adv Mater. 2011;23:884–888.
[4] Manda R, Pagidi S, Bhattacharyya SS, et al. Fast response and transparent optically isotropic liquid crystal diffraction grating. Opt Express. 2017;25:24033–24043.
[5] Manda R, Pagidi S, Kim MS, et al. Effect of monomer concentration and functionality on electro-optical properties of polymer-stabilised optically isotropic liquid crystals. Liq Cryst. 2018;45:736–745.
[6] Shi Z, Wang Y, Wang Y. Effects of thiol monomers on the electro-optical properties of polymer-dispersed liquid crystal films prepared by nucleophile-initiated thiol-ene click reaction. Liq Cryst. 2018;45:1746–1752.
[7] Bouriche A, Alachaher LB, Maschke U. Phase behaviour and electro-optical response of systems composed of nematic liquid crystals and poly (2-ethylhexylacrylate). Liq Cryst. 2018;45:656–665.
[8] Liu YJ, Sun XW, Liu JH, et al. A polarization insensitive 2 × 2 optical switch fabricated by liquid crystal-polymer composite. Appl Phys Lett. 2005;86:041115.
[9] Liu YJ, Sun XW, Shum P, et al. Tunable fly's-eye lens made of patterned polymer-dispersed liquid crystal. Opt Express. 2006;14:5634–5640.
[10] Liu YJ, Sun XW. Electrically switchable computer-generated hologram recorded in polymer-dispersed liquid crystals. Appl Phys Lett. 2007;90:191118.
[11] Liu YJ, Sun XW, Wang Q, et al. Electrically switchable optical vortex generated by a computer-generated hologram recorded in polymer-dispersed liquid crystals. Opt Express. 2007;15:16645–16650.
[12] Liu YJ, Dai HT, Sun XW, et al. Electrically switchable phase-type fractal zone plates and fractal photon sieves. Opt Express. 2009;17:12418–12423.
[13] Chien C-Y, Hsu C-J, Chen Y-W, et al. Holographic polymer networks formed in liquid crystal phase modulators via a He-Ne laser to achieve ultra-fast optical response. Opt Express. 2016;24(7):7534–7542.
[14] Zhou P, Li Y, Li X, et al. Holographic display and storage based on photo-responsive liquid crystals. Liq Cryst Rev. 2016;4:83–100.
[15] Huang S, Li Y, Zhou P, et al. Polymer network liquid crystal grating/Fresnel lens fabricated by holography. Liq Cryst. 2017;44:873–879.

[16] Li H, Qi Y, Guo C, et al. Holographic characterization of diffraction grating modulation in photopolymers. Appl Opt. 2018;57:E107–E117.
[17] Gruber HF. Photoinitiators for free radical polymerization. Prog Polym Sci. 1992;17:953–1044.
[18] Vaz NA, Smith GW, Montgomery GP. A light control film composed of liquid crystal droplets dispersed in a UV-curable polymer. Mol Cryst Liq Cryst. 1987;146:1–15.
[19] Drzaic PS. Polymer dispersed nematic liquid crystal for large area displays and light valves. J Appl Phys. 1986;60:2142–2148.
[20] Parshin AM, Gunyakov VA, Zyryanov VY, et al. Domain structures in nematic liquid crystals on a polycarbonate surface. Int J Mol Sci. 2013;14:16303–16320.
[21] Kumaki J, Hashimoto T, Granick S. Temperature gradients induce phase separation in a miscible polymer solution. Phys Rev Lett. 1996;77:1990–1993.
[22] Lee K-WD, Chan PK, Feng X. A computational study into thermally induced phase separation in polymer solutions under a temperature gradient. Macromol Theory Simul. 2002;11:996–1005.
[23] Matsuyama H, Kakemizu M, Maki T, et al. Preparation of porous poly(oxymethylene) membrane with high durability against solvents by a thermally induced phase-separation method. J Appl Polym Sci. 2002;83:1993–1999.
[24] Ren H, Wu S-T, Lin Y-H. In situ observation of fringing-field-induced phase separation in a liquid-crystal–monomer mixture. Phys Rev Lett. 2008;100:117801.
[25] Kitzerow H-S. Polymer-dispersed liquid crystals from the nematic curvilinear aligned phase to ferroelectric films. Liq Cryst. 1994;16:1–31.
[26] Olivier A, Pakula T, Best A, et al. A static and dynamic study of the mechanical properties of electron beam cured PDLC films. Mol Cryst Liq Cryst. 2004;412:2071–2077.
[27] Dai HT, Chen L, Zhang B, et al. Optically isotropic, electrically tunable liquid crystal droplet arrays formed by photopolymerization-induced phase separation. Opt Lett. 2015;40:2723–2726.
[28] Park S-J, Lee J-R. Dispersive stabilization of liquid crystal-in-water with acrylamide copolymer/surfactant mixture: nematic curvilinear aligned phase composite film. J Colloid Interf Sci. 1999;219:178–183.
[29] De Sio L, Lloyd PF, Tabiryan NV, et al. Hidden gratings in holographic liquid crystal polymer-dispersed liquid crystal films. ACS Appl Mater Interfaces. 2018;10:13107–13112.
[30] Shanks RA, Staszczyk D. Thermal and optical characterization of polymer-dispersed liquid crystals. Int J Polym Sci. 2012;2012:767581.
[31] Li Y, Huang S, Zhou P, et al. Polymer-stabilized blue phase liquid crystals for photonic applications. Adv Mater Technol. 2016;1:1600102.
[32] Dierking I. Polymer network-stabilized liquid crystals. Adv Mater. 2000;12:167–181.
[33] Vorflusev V, Kumar S. Phase-separated composite films for liquid crystal displays. Science. 1999;283:1903–1905.
[34] Avci N, Hwang S-J. Electrically tunable polarisation-independent blue-phase liquid crystal binary phase grating via phase-separated composite films. Liq Cryst. 2017;44:1559–1565.
[35] Lin H-Y, Avci N, Hwang S-J. High-diffraction-efficiency Fresnel lens based on annealed blue-phase liquid crystal-polymer composite. Liq Cryst. 2019. DOI:10.1080/02678292.2018.1562114
[36] Kajiyama T, Nagata Y, Washizu S, et al. Characterization and gas permeation of polycarbonate/liquid crystal composite membrane. J Memb Sci. 1982;11:39–52.
[37] Zumer S, Doane JW. Light scattering from a small nematic droplet. Phys Rev A. 1986;34:3373–3386.
[38] Zumer S. Light scattering from nematic droplets: anomalous-diffraction approach. Phys Rev A. 1988;37:4006–4015.
[39] Doane JW, Golemme A, West JL, et al. Polymer dispersed liquid crystals for display application. Mol Cryst Liq Cryst. 1988;165:511–532.
[40] Wu B-G, Erdmann JH, Doane JW. Response times and voltages for PDLC light shutters. Liq Cryst. 1989;5:1453–1465.
[41] Petti L, Mormile P, Blau WJ. Fast electro-optical switching and high contrast ratio in epoxy-based polymer dispersed liquid crystals. Opt Laser Eng. 2003;39:369–377.
[42] Liu YJ, Sun XW. Electrically tunable two-dimensional holographic photonic crystals fabricated by a single diffractive element. Appl Phys Lett. 2006;89:171101.
[43] Liu YJ, Sun XW. Electrically tunable three-dimensional holographic photonic crystals made of polymer-dispersed liquid crystal. Jpn J Appl Phys. 2007;46:6634–6638.
[44] Liu YJ, Zheng YB, Shi J, et al. Optically switchable gratings based on azo-dye-doped, polymer-dispersed liquid crystals. Opt Lett. 2009;34:2351–2353.
[45] Liu YJ, Dai HT, Leong ESP, et al. Electrically switchable two-dimensional photonic crystals made of polymer-dispersed liquid crystals based on the Talbot self-imaging effect. Appl Phys B. 2011;104:659–663.
[46] Liu YJ, Ding X, Lin S-CS, et al. Surface acoustic wave driven light shutters using polymer-dispersed liquid crystals. Adv Mater. 2011;23:1656–1659.
[47] Qian T, Kim J-H, Kumar S, et al. Phase-separated composite films: experiment and theory. Phys Rev E. 2000;61:4007–4010.
[48] Aizumi S, Shirao M, Yamamuro Y, et al. Effect of wettability on fabrication of PSCOF liquid crystal cell. Mol Cryst Liq Cryst. 2015;608:258–263.
[49] Kumar S, Kim J-H, Shi Y. What aligns liquid crystals on solid substrates? The role of surface roughness anisotropy. Phys Rev Lett. 2005;94:077803.
[50] Guo S, Liang X, Zhang H, et al. An electrically light-transmittance-controllable film with a low-driving voltage from a coexistent system of polymer-dispersed and polymer-stabilised cholesteric liquid crystals. Liq Cryst. 2018;45:1854–1860.
[51] Song P, Cao H, Wang F, et al. The UV polymerisation temperature dependence of polymer-dispersed liquid

crystals based on epoxies/acrylates hybrid polymer matrix components. Liq Cryst. 2012;39:1131–1140.
[52] Yin D, Pu H, Gao B, et al. Analytical rates determinations and simulations on diffusion and reaction processes in holographic photopolymerization. Appl Phys Lett. 2009;94:211108.
[53] Wang Q, Park JO, Srinivasarao M, et al. Control of polymer structures in phase-separated liquid crystal-polymer composite systems. Jpn J Appl Phys. 2005;44:3115–3120.
[54] Allen SM, Chan JW. Ground state structures in ordered binary alloys with second neighbor interactions. Acta Metall. 1972;20:423–433.
[55] Diekmann K, Schumacher M, Stegemeyer H. Nucleus growth in liquid crystals. Liq Cryst. 1998;25:349–355.